Morphometry of cellular behavior of coelomocytes from starfish *Asterias amurensis*

Yuriy A Karetin [Corresp. 1]

[1] A.V. Zhirmunsky National Scientific Center of Marine Biology, Far Eastern Branch, Russian Academy of Sciences, Vladivostok, Russia

Corresponding Author: Yuriy A Karetin
Email address: yura15cbx@gmail.com

A comprehensive statistical analysis using a wide range of linear and non-linear morphological parameters enabled identification of the main stages in the *in vitro* dynamics of cell behavior of immune cells of the marine invertebrate *Asterias amurensis* (Echinodermata, Asteroidea). Three stages may be distinguished in the cell behavior, which are characterized by the differences in complexity of the cell boundary microsculpture as well as by the size and asymmetry of the cell and convex hull of the cell. The first stage (5 min after placing cells onto a substrate) is characterized by more complex cell morphology and an increase in the process number and spreading area. The second stage (15 min) is characterized by simplification of cell morphology, retraction of some processes, and rounding of cells upon continued cell spreading. At the third stage (60 min), new large processes with rounded contours emerge due to partial retraction of the flattened cell surface. Each stage is characterized by statistically significant differences in several linear and nonlinear parameters of the external morphology for all cell types.

Morphometry of cellular behavior of coelomocytes from starfish Asterias amurensis

Yuriy Karetin

A.V. Zhirmunsky National Scientific Center of Marine Biology, Far Eastern Branch, Russian
Academy of Sciences. Palchevskogo Str, 17, Vladivostok, Russia, 690041
Email address: yura15cbx@gmail.com

Abstract

A comprehensive statistical analysis using a wide range of linear and non-linear morphological parameters enabled identification of the main stages in the *in vitro* dynamics of cell behavior of immune cells of the marine invertebrate *Asterias amurensis* (Echinodermata, Asteroidea). Three stages may be distinguished in the cell behavior, which are characterized by the differences in complexity of the cell boundary microsculpture as well as by the size and asymmetry of the cell and convex hull of the cell. The first stage (5 min after placing cells onto a substrate) is characterized by more complex cell morphology and an increase in the process number and spreading area. The second stage (15 min) is characterized by simplification of cell morphology, retraction of some processes, and rounding of cells upon continued cell spreading. At the third stage (60 min), new large processes with rounded contours emerge due to partial retraction of the flattened cell surface. Each stage is characterized by statistically significant differences in several linear and nonlinear parameters of the external morphology for all cell types.

Introduction

Asterias amurensis is a seastar native to the seacoasts of China, Korea, Russia and Japan. This species recently has been introduced to the Tasmania, southern Australia, Alaska, the Aleutian Islands, parts of Europe, and Maine (Stevens, 2012). Today the species attracts the close attention of researchers in view of the wide spread, threatening the stability of biocenoses on the introduced territories (Ross et al., 2002; Dommisse and Hough, 2004).

The typical parameters for classification of invertebrate immune cells include features such as the cytoplasm granularity, nuclear-cytoplasmic relationships, phagocytic activity and immunological specificity. Most of these features are variable (Fisher, 1986). For example, granulocytes may have the agranular precursors (Hine, 1999); according to Martin and Hose (1992), granules can appear upon condition changes or be present in cells defined as hyalinocytes based on other morphological features. The ability of marine invertebrate immune cells to phagocytosis can significantly differ among animals within a single population (Kurtz, 2002); phagocytosis can be observed only in one type (Scapigliatia and Mazzinia, 1994) or in all described types of hemocytes (Stoepler et al., 2013). Invertebrates also may mount a highly variable immune response that is dependent on which pathogen is involved (Cerenius and Söderhäll, 2013). The antigens characterize distinct subsets which partially overlap with those defined by morphological description (Kurucz et al., 2007). In some species only individual cell types became immunologically activated with obvious morphological changes (Hwang et al, 2015).
Since the conventional parameters often provide an ambiguous picture, the development of a universal classification scheme requires a combination of more extensive morphometric, genetic

83 and biochemical methods as well as cytodifferentiation data of determining the cell specificity.
84 Different sets of parameters will potentially able to identify different cell types associated with a
85 particular feature of their physiology or morphology. Which of classification models can serve as
86 a natural universal model for the classification hemocytes it is still an open question. However,
87 we may suppose that the external morphology play an important role in the natural classification
88 of invertebrate immune cells. Features of morphology of the flattened cell shape are reflected in
89 its cytoskeleton structure, the organization of related cell systems and directly dependent on the
90 type-specific cell behavior.
91   The methodology of multiparametric morphological classification of immune cells of
92 invertebrates, using nonlinear parameters of morphology analysis (Karetin, 2010, 2015) and
93 interspecific comparisons of morphotypes of invertebrate cells based on such a methodology
94 (Karetin, 2016) show their effectiveness in describing the morphology of hemocytes and
95 coelomocytes of marine invertebrates. However, a description of static cell morphology, which is
96 usually carried out in a few minutes after the attachments, makes classification schemes based on
97 morphological features incomplete. Analysis of the dynamics of cellular behavior shows that we
98 are dealing with a number of transitional forms, the dynamics of which can also reflect the
99 species-specific features of cellular behavior, the state of the animal's immune status or reaction
100 to the experimental effect. Description of cell dynamics should complement the static patterns of
101 cellular morphology used for description of the cellular immunity of invertebrates.
102   Using the population of Asterias amurensis coelomocytes as example, we have shown in
103 this work the effectiveness of multiparametric analysis of the dynamics of the spreading of
104 immune cells, with the identification of a number of characteristic morphotypes of cells and their
105 transformation in the process of short-term cultivation.
106
107

108 **Materials & Methods**
109
110   *Material preparation*
111   The study was performed on 398 coelomocytes of the 10 *Asterias amurensis* starfish
112 (Echinodermata, Asteroidea) (Lutken, 1871). Field experiments were approved by the Federal
113 Fisheries Administration, Primorsky Territorial Administration, issued for NSCMB FEB RAS.
114 Approval number to access field sites: 252021030802. Animals were collected in the Peter the
115 Great Bay (Sea of Japan, Russia). After collecting, the coelomic fluid was sampled from the
116 starfish coelomic cavity using a syringe, placed onto glass coverslips, and incubated for 2, 5, 15,
117 and 60 min. After incubation the glasses with adhered cells were fixed with a 4% formaldehyde
118 solution in seawater, stained with hematoxylin and eosin, dehydrated, and embedded in Canada
119 balsam for a light microscopy study. Photos of the adhered cells were taken using a 10-
120 megapixel digital camera of a Zeiss Axiovert 200M Apotome microscope (magnification of the
121 x100 lens). The images of the cells were drawn directly from a tablet computer screen onto
122 transparent films that were then scanned. Both silhouette and contour images of flattened cells

123   were analyzed. A single pixel outline of the outer cell boundary was used for contour images.
124   Cell images were digitized and converted to single-bit format.
125   *Parameterization*
126   Parameters were obtained using ImageJ 1.41 image analysis software with a FracLac 2.5
127   plug-in for a fractal analysis. 1/2half и in50/out50 was calculated using a program CellMaster
128   1.3.2b, https://figshare.com/s/d3c3784e43efa1913db4, author: Eduardas Cicinskas.
129   A total of 39 parameters were examined (see Supplemental 1); of these, 19 parameters
130   were selected for use, including 7 nonlinear and 12 linear parameters.
131   Linear parameters:
132   *Aspect ratio*: major_axis/minor_axis of cell image, (***AR***);
133   *Roundness*: 4*area /(π*major_axis^2), (***Round***);
134   ***1/2half***: the ratio of area parts of the cell in the two halves of the bounding circle. The
135   diameter dividing cells was drawn in the direction that most unevenly divided the image of cells.
136   Parameter was used as a measure of cell asymmetry;
137   ***in50/out50***: The ratio of cell area in the outer half of the bounding circle to the area of the
138   cells in the inner half of bounding circle;
139   ***Area***;
140   *Circularity*: 4π*area / perimeter^2, (***Circ***);
141   *Feret's Diameter*: the longest distance between any two points along the object boundary,
142   also known as maximum caliper, (***Feret***);
143   *Hull's Perimeter*: perimeter of the convex hull drawn around the object. The convex hull
144   is a boundary enclosing the foreground pixels of an image using straight line segments to each
145   outermost point, (***Hull'sPer***);
146   *Diameter of Bounding Circle*: the smallest circle around the convex hull,
147   (***DiamBoundCirc***);
148   ***Density***: Foreground Pixels/Hull Area;
149   *Perimeter* of cell, (***Per***);
150   *Hull's Perimeter*: perimeter of the convex hull drawn around the object (Hull'sPer);
151   Nonlinear parameters:
152   Lacunarity L (F - foreground pixels): lacunarity based on the variation of pixels in each
153   analyzed box summarized over all grid orientations for an image, only pixels of the image of the
154   object were taken into account, (***LF***);
155   Lacunarity L (E - foreground and empty space): lacunarity calculated on the basis of
156   differences in the number of pixels in each square of the grid for all orientations of the squares,
157   with allowance for the background pixels taken as zero, (***LE***);
158   ***outMeanΛD***: The lacunarity of contour images of cells based box counting dimension
159   (ΛD_B) or its average $\Lambda D_B = (Grids\sum G{=}1(\Lambda D_{B(G)}))\times Grids^{-1}$, where $\Lambda D_{B(G)}$ is the lacunarity
160   calculated for each orientation of the grid, Grids are all possible orientations of the grid;
161   ***MeanΛ***: Average lacunarity calculated for different orientations of the square grid;

162   *LCFD Prefactor Lacunarity*: a measure of heterogeneity or translational invariance
163   dependent on where a grid series is placed, Local Connected Fractal Dimension is found from a
164   type of fractal analysis that uses pixel mass from concentrically placed sampling units, using
165   the connected set around each pixel to produce a distribution of local variation in complexity,
166   (**LCFD PreLac**);
167   Fractal dimension of contour images of cells calculated as follows: *Mean D*
168   =Σ(D)/GRIDS (D=slope (ln(Boxes with Foreground Pixels)/ln(ε)), where ε - box size or scale,
169   the average D_B (box-counting fractal dimension) from multiple box counting scans, each
170   delivering its own D_B, based on a different orientation of grid, (**outMeanD**);
171   *Mean Local Fractal Dimension*: the average dimension calculated on the basis of
172   multiple sampling an image and defining the local fractal dimension of various parts of contour
173   images of cells, (**outMeanLFD**).
174
175   *Statistical analysis.*
176   All analyses were performed using NCSS 2007 and STATISTICA 10 software.
177   The correlation between parameters was measured using Pearson's linear correlation analysis.
178   The scatterplots of pair-wise correlations were also examined to reveal false correlations due to
179   outliers (Gordon, 1999). In each group of significantly correlated parameters (R ≥ 0.8 at p <
180   0.05), only one parameter was selected to assure that the respective aspect of cell morphology is
181   adequately, but non-redundantly, represented (Schweitzer and Renehan, 1997).
182   Cells were classified using a hierarchical cluster analysis; the Ward's agglomerative algorithm
183   providing the best results in classifying cell objects on the basis of morphological parameters
184   was used as a clustering method (Pushchin and Karetin, 2009). It starts with each object as a
185   separate cluster, merging similar objects into successively larger clusters. Analysis of variance is
186   used at each cycle to minimize the within-cluster variance.
187   Tukey-Kramer Multiple-Comparison Test is a single-step multiple comparison procedure
188   that was used to find means of groups that are significantly different from each other. It
189   compares all pairs of means, and is uses a studentized range distribution (q).
190
191
192

193 **Results**

194

195   *Visual description of cell morphology*
196   Two minutes after placing cells onto glass (group 1), cells that could spread and form a
197   large number of small and large processes were observed among a large number of small cells
198   with minor processes. Cells fixed 5 min after placement (group 2) were the most heterogeneous
199   group in the experiment. The group included both small cells with minor processes and cells of a
200   very complex structure, with long processes covered by secondary microprocesses, branched
201   processes, and processes with expanding ends. After 15 min of culturing (group 3), cells

202 remained visually very flattened, but acquired in most cases a more regular nonsegmented shape
203 compared to cells of the previous group. Often, their shape was nearly round; the cells had a
204 small number of thin and long processes or a large number of small processes evenly covering
205 the outer contour of the cell. After 60 min of culturing (group 4), the number of small cellular
206 processes was visually even more reduced; the processes lost sharpness; the microsculpture of
207 cell boundaries became simpler; rounded cell forms at this stage alternated with cells having a
208 small number of large processes (Fig 1). At this stage, a morphotype emerged that had been
209 absent at the earlier cultivation times: cells with curved, circle segment-like processes.
210 Therefore, starting with the 15th min of culturing, simplification of the cell morphology and
211 retraction of small processes occurred along with continued cell spreading. At the 60th min of
212 culturing, retraction led to the disappearance of certain cell regions: there remained elements of
213 the region boundary in the form of curved pseudopodia delineating the boundary.
214    *Trends in parameter dynamics*
215    The dynamics of cultured cell parameters demonstrated 5 trends: 1. an increase or drop in
216 the parameter value during culturing, with a significant difference of each group (ex. Area) (Fig.
217 2A); 2. a sharp decrease or increase in the studied parameter value in group 2 (ex. Circularity)
218 (Fig. 2B); 3. a significant increase in the parameter value in the period from the 2nd to 5th min
219 and from 15th to 60th min of culturing, with an insignificant difference between groups 2 and 3
220 (ex. Feret's diameter) (Fig. 2C); 4. an increase or decrease in the parameter value, starting with
221 group 3, with an insignificant difference between groups 1 and 2 (ex. outMeanLCFD) (Fig. 2D);
222 5. significantly smaller parameter values in groups 1 and 3 and significantly larger parameter
223 values in groups 2 and 4 (ex. in50/out50) (Fig. 2E). A wide range of parameters had no
224 significant differences among all four groups.
225    Parameters showing similar trends were usually highly correlated, although there were
226 exceptions from this rule. Parameters, changes in which during culturing had no recognizable
227 trends, were not of great interest for this study because they did not reflect the dynamics of
228 morphological transformations of cultured cells; although, different cell types within a single
229 time group showed significant differences in some parameters (AR, Round), and some of these
230 parameters (e.g., 1/2half) became key parameters for classifying cells within the same time group
231 in other species of marine invertebrates (Karetin and Pushchin, 2015). In general, according to
232 the Tukey-Kramer multiple comparison test, cells of all 4 time groups had significant differences
233 in a number of studied parameters (Table 1).
234    *Peculiarities of parameter selection*
235    A parameter selection methodology used in our previous studies (Pushchin and Karetin,
236 2014; Karetin and Pushchin, 2015) involved the initial search for highly correlated
237 characteristics and selection of those that had a higher multimodality index value. In the present
238 study, the methodology needed modifying because characteristics highly correlated in the same
239 time group were not correlated in another, and many parameters with similar trends in parameter
240 value changes had almost identical multimodality indices that differed by no more than 0.01.
241 Parameters with a lower multimodality index were excluded from the parameters highly

242   correlated in all 4 time groups as well as from the parameters with similar trends. In the case of
243   similar multimodality indices, we chose a parameter providing a better cluster structure of
244   identified cell types; highly correlated parameters with a similar trend in the parameter dynamics
245   as well as parameters without significant differences in all time groups were excluded from the
246   cluster analysis and description of intergroup differences.

247   The lack of correlation for similar trends and *vice versa* as well as the difference in
248   correlation in different time groups generally indicate that this parameter in different cell groups
249   describes different features of cell morphology.

250   *Characteristics of cell morphology described by the parameters used.*

251   A complex of linear and quasi-fractal parameters was used to parametrize the cells.
252   Linear parameters include morphometric parameters based on Euclidean geometry, such as the
253   area, the perimeter of the cell, a number of parameters of the bounding circle and the convex
254   hull. The area reflects the size of the cell and, to a greater extent, the spreading area, which can
255   be many times larger than the original size of the cell, the perimeter depends on both the size of
256   the cell and the number of processes, the bounding circle and the convex hull (a boundary
257   enclosing the foreground pixels of an image using straight line segments to each outermost point,
258   Fig. 3) reflect the area of cell stratification defined by the longest processes. Also, the linear
259   parameters include density, which reflects the ratio of the number of pixels in the image to the
260   total number of pixels covered by the circle bounding the cell. The value of *density* depends on
261   the ratio of the size of the cell body to the area of stratification of its processes.

262   The parameters *Roundness* and *Circularity* characterize various aspects of the cell shape,
263   Roundness characterizes the deviation of the shape of the object from the circle towards the
264   ellipse; Circularity, determined by the ratio of the area to the perimeter, is equal to one for the
265   circle and decreases as the perimeter of the cell border increases, that is, it depends not only on
266   the overall shape, as in the case of Roundness, but also on the number of cell processes that
267   increase the perimeter of the cell.

268   The parameter 1/2half is the ratio of area parts of the cell that turned out to be in the two
269   halves of the bounding circle most unevenly divided the image (in Figure 4: 1/2half = A/B). The
270   largest values of this parameter will belong to the cells most asymmetrically positioned inside the
271   bounding circle. The in50/out50 parameter describes the ratio of the cell area in the inner and
272   outer parts of the bounding circle (in Figure 4: in50/out50 = C/D), the parameter value is
273   determined both by the asymmetry of the cell location inside the bounding circle, and by the
274   ratio of the cell body size and the area of stratification of the cell processes.

275   Nonlinear parameters include a number of fractal dimensions and lacunarities, the value
276   of which depends on the complexity of the object or the heterogeneity of its space filling. Fractal
277   analysis is based on the consideration of an object as a quasi-fractal, which has a fractional
278   dimension, the values that describe them are the same as objects of Euclidean geometry
279   describes by measures of length, area, or volume. The basic algorithm for calculating the fractal
280   dimension used here is the box-counting method, for counting which an object is enclosed in a
281   network of squares of a certain size (Fig. 5). The number of squares that the structure fell into is

282 calculated, and the ratio of the decimal logarithm of the number of squares that covered the
283 structure to the decimal logarithm of the length of the side of the square is determined. In the
284 next step, the structure is covered by a network of smaller squares. Again, we calculate the ratio
285 of the logarithms of the number of squares and the length of their sides. We do this procedure
286 several times. The resulting dimension value is calculated using the formula:

287   ln N (L)
288 D = lim ---------
289   (L → 0)   ln L

290   Where N (L) is the number of squares with side L required to cover the fractal structure.
291 Different types of fractal dimensions have a similar basic algorithm and can differ in such
292 aspects as the shape of the elements in which the object is enclosed (it may not be a square grid,
293 but a set of circles of increasing diameter, *mass-radius dimension*), the location of the grid
294 elements: fixed squares or a rotating grid (*MeanD*), the calculation can be performed for the
295 entire image as a whole (*MeanD*), or the local dimension in the vicinity of each pixel (*Local
296 fractal dimension*) is calculated and averaged. To calculate the dimension of only the upper and
297 lower scale of the image, only a large (*BiggestD*) or small (*SmallestD*) grid is used, respectively.
298 The fractal dimension in our work was measured in contour and silhouette images. Silhouette
299 images represent a planar one-bit image of a flattened cell, in the contour image only the one-
300 pixel contour of the silhouette image of the cell remains. The fractal dimension of silhouette and
301 contour images is significantly different, since the value of the fractal dimension of the silhouette
302 image increases by the space filled with image pixels inside the cell, while the fractal dimension
303 of contour images consists only of the fractalization of the cell boundaries.
304 Twofold increase the complexity of the cell shape leads to an increase in its fractal dimension by
305 about 0.1 (Jelinek and Fernandez, 1998). Different types of fractal dimensions describe different
306 aspects of the complex shape of a flattened cell. These differences are difficult to formalize in
307 traditional terms of Euclidean geometry or classical descriptions of cell morphology, but they
308 reliably differentiate different cell types.
309   *Cell types*
310   Because the visual analysis revealed that cells of each time groups were a
311 morphologically heterogeneous population, cells of all groups were divided into morphotypes
312 using a hierarchical cluster analysis. Five weakly correlated parameters with different trends in
313 the parameter dynamics during culturing were selected for the cluster analysis: Area, Circ, Feret,
314 in50/out50, and LE. The parameters were used to generate a cluster model for each time group,
315 which clearly revealed three clusters corresponding to three cell morphotypes (Fig. 6). Four
316 clusters might be distinguished in a cell sample from group 3; however, 3 clusters were also
317 chosen in this group to simplify intergroup comparisons. This is consistent with the logic of
318 hierarchical cluster analysis when closely related types can always be combined into a common
319 parent type; cells of the parent type combine characteristics of subsidiary cell types and, to the
320 same or greater extent, differ from cells of other clusters, like cells of subsidiary clusters.

321   Cells of obtained types differed in a number of the analyzed parameters. In this case, similarity
322   of trends in parameter changes among types in each time group suggested that the cluster
323   analysis identified a similar cell types in each group by transposing types 1 and 2 in the second
324   group, which did not change the general picture because a cluster sequence may be arbitrary due
325   to free rotation of cluster axes, not affecting results of the cluster analysis. In general, the
326   identified cell types are characterized by different sizes and complexity of cell boundaries. Here,
327   we may distinguish small cells with simple boundary microsculpture: 2-1, 5-2, 15-1, and 60-1
328   (type I); medium-sized cells: 2-3, 5-3, 15-3, and 60-3 (type II); large cells or cells with very
329   complex dendritic microsculpture of boundaries: 2-2, 5-1, 15-2, and 60-2 (type III) (Fig. 7).
330   The parameter Area most clearly distinguished both time groups and individual cell types within
331   time groups (Fig. 8a). It is seen that cell types include the smallest (type I), medium (type II), and
332   large (type III) cells. In this case, the area of cells of similar types in different time groups
333   increases within the 2 to 60 min culturing interval. Because we consider a single population of
334   cells, this indicates that the spreading process that is accompanied by an increase in the area of
335   the two-dimensional cell projection occurs in all cell types throughout the cultivation period.
336   When considering trends of individual cell types, parameters that are correlated with Feret's
337   Diameter, characterized by trend 3, and have an insignificant difference between time groups 2
338   and 3 demonstrate a continuous increase in the parameter value, with significant differences
339   among all cell types within each group; however, group 3 has a lower upper boundary for feature
340   manifestation compared to that of group 2, with the lower boundary being higher, which makes
341   group 3 comparable to group 2 in the mean feature value (Fig. 8b). The Feret's diameter is a
342   dimensional characteristic correlated with parameters of the convex hull and bound circle, such
343   as Hull'sPer and DiamBoundCirc. Both the total cell area and processes size affect values of all
344   these parameters. An increase in the total cell area, which is well detectable in small type I cells
345   with minor processes, is compensated by a decrease in complexity of cell boundaries in type II
346   and III cells of group 3, which creates the effect of absent significant differences in these
347   parameters between groups 2 and 3.
348   A group of parameters demonstrating a sharp drop or increase in a studied parameter
349   value in group 2 (trend 2), which includes parameters Circularity, Density, and LF, demonstrates
350   a small increase or decrease in parameter values upon transition from the Ist to IIIrd cell type. In
351   this case, confidence intervals of values in most cases overlap both among cell types of the same
352   group and among different time groups. The exceptions are cell types 5-3 and 5-1 that sharply
353   distinguish group 2 from other groups. Decreased circularity and cell image density and
354   increased lacunarity always non-specifically characterize an increase in structural complexity of
355   the cell, cell protrusivity, complexity of boundaries, elongation, and asymmetry of filling of the
356   surrounding space by the cell. The same pattern is observed for parameters associated with trend
357   5 (Perimeter, in50/out50): upon similar parameter dynamics for most cell types, types 5-1 and 6-
358   2 are characterized by a sharp increase in values of the parameters Perimeter and in50/out50,
359   which also indicates increased protrusivity in these cell types (Fig. 8c).

360 In general, it is noteworthy that the cell type 5-1 significantly surpasses the other cell
361 types in most parameters that directly (several nonlinear parameters: outMeanLD, LF, MeanL,
362 LCFD PreLac) or indirectly (several linear parameters: Circ, Density, in50/out50, Per)
363 characterize spatial complexity of the cell. It is the type that includes cells reaching the highest
364 level of spatial complexity at the 5th minute.
365 Parameters based on measurements of the convex hull and bound circle (Hull'sPer,
366 DiamBoundCirc) (Fig. 8d) combine characteristics of cell size and the degree of protrusivity and
367 are reducible to characteristics of filling of the surrounding space by the cell. Two cell types are
368 clearly distinguished by high values of these parameters: 5-1 − cells with the highest degree of
369 protrusivity and 60-2 − cells with the largest area and protrusivity that reduces to the 15th min of
370 culturing and re-emerges at the 60th min, which is associated with partial retraction of the
371 flattened cell body leaving large curved processes, as described above.
372 In addition, it can be seen that cell types 15-2 and 60-2 are significantly different in
373 parameters Hull's Circularity and Roundness (Fig. 8e); the other cell types do not have
374 significant differences in these parameters. The Roundness describes similarity of the overall cell
375 shape to the circle ($4*area/(\pi*major\_axis$ of fitted ellipse^2), i.e. the highest Roundness value is
376 observed for cells with an elongated shape typical of crawling cells or cells with long
377 asymmetrically arranged processes. Large errors of the parameter's mean and the absence of
378 significant differences among most of the cell types indicate that a chaotic variety of common
379 cellular shapes does not reflect any structural and functional patterns occurring in cell culture by
380 the 15th minute of culturing. Only a significant increase in this parameter in types 15-2 and 60-2
381 at the 15th and 60th minutes of culturing means rounding of cells, which indicates the
382 disappearance of large processes and a reduction in cell motility that leads to the development of
383 radial symmetry. Also, rounding of cells is reflected in an increase in the Hull's Circularity
384 parameter value. The Circularity parameter that is based on the ratio of the object perimeter to
385 the object area ($4\pi*area/perimeter^2$) reduces as the perimeter increases, i.e. it is anti-correlated
386 with many nonlinear parameters that increase as indentation of cell boundaries becomes more
387 pronounced, which is confirmed by the correlation analysis. However, Circularity applied to the
388 convex hull connecting only extreme points of an object becomes a parameter that characterizes
389 the overall shape of the object.
390 *Correlation analysis*
391 Interestingly, the presence of significant correlations for some pairs of parameters only in
392 the 2nd time group is related to the prevalence of cells with much more complex morphology
393 (type 5-1) in this group compared to other groups. For example, two parameters: Area −
394 outMeanD (0.01, **0.70**, 0.05, and 0.18; correlations are provided for groups 1−4, respectively;
395 significant and high correlations are shown in bold) demonstrate a significantly high correlation
396 in the second group because a simultaneous significant increase in the area and spatial
397 complexity of the cell occurs only in this group. A variety of both large and small cells with
398 simple microsculpture (and, correspondingly, with a lower outMeanD value) makes the
399 correlation between these parameters in other groups insignificant. We observed the same effect

400   of spatial complexity of the cell contour on correlation of characteristics in a pair of
401   characteristics: Feret − Density (−0.14, **−0.80**, −0.30, −0.58). An increase in Feret, a parameter
402   describing one of the characteristics of space filling by the cell, is anti-correlated with Density
403   only if an increase in the filling area is achieved through an increase in the length and number of
404   cellular processes (and, correspondingly, through a decrease in the ratio of the number of object
405   pixels to the number of background pixels), but not through continuous filling of the space by the
406   cell body; otherwise, these two parameters are positively correlated. In other groups, an increase
407   in the Feret value is achieved both through an increase in the size of flattened cells and through
408   an increase in the number of processes, which makes the correlation invalid.
409   Some parameters have sufficient discriminatory power for reliable identification of the
410   most dendritic cells combined in types 5-1 and 60-2. These parameters also form variable
411   correlations in different time groups. One of these pairs is Density − Perimeter (0.31, **−0.76**,
412   −0.42, **−0.70**). In groups 2 and 4, low density of the cell image in dendritic cells with a high
413   degree of cell boundary indentation is anti-correlated with a large length of the cell perimeter; in
414   groups 1 and 3, whose cells have less complex morphology, the density and perimeter grow
415   simultaneously as the cell size increases, due to continuous filling of the surrounding space by
416   the cell body, which makes the correlation insignificant.
417   In some cases, the difference in correlation in different time groups is associated with
418   different dynamics of parameter changes in cells with different morphology. For example, in a
419   pair of parameters outMeanD − outMeanLFD (**0.73**, 0.21, **0.66**, 0.34), only the parameter
420   outMeanD grows as protrusivity strongly increases in cells of groups 2 and 4; outMeanLFD is
421   not correlated with the maximum increase in spatial complexity of the cell; the greatest
422   outMeanLFD value occurs in a special type of cells with a relatively uniform distribution of
423   processes around the cell body (Fig. 9). The morphology of these cells can be called moderately
424   complex, and outMeanD values of these cells are medium. In groups 1 and 3, where this cell type
425   reaches the maximum complexity of cell morphology, outMeanLFD is correlated with
426   outMeanD; in groups with a sufficient number of cells with higher spatial complexity, a further
427   increase in the outMeanD parameter is not accompanied by an increase in the outMeanLFD
428   parameter, and the correlation is not valid.
429
430

431   **Discussion**

432

433   Coelomic fluid cells in invertebrates perform the protective function that is realized
434   through several variants of a single systemic cellular response to a foreign body: phagocytosis of
435   microscopic foreign particles identified by the cell, encapsulation − in vivo cell spreading across
436   a foreign body that is too big to be uptaken by the cell, and, finally, cell spreading through a
437   substrate as an attempt to isolate the foreign surface, the amount of which significantly exceeds
438   the cell size (Ratner and Vinson, 1983).
439   Within a few minutes after placing coelomic fluid onto an artificial substrate, cells

440 precipitate, adhere to it, form conglomerates of various sizes (a reaction of thrombus formation
441 and cell agglutination of a body fluid, which is transferred to *in vitro* condition) and flatten. In
442 this case, some species form almost a continuous cell layer, while others form a network of
443 contiguous pseudopodia of cells self-assembled into cell flows.
444   Morphological characteristics of coelomocytes vary greatly in different species of
445 echinoderms, even within the same class. In the late 1950s, R.A. Boolootain and A.C. Guise
446 from the Stanford University, on the basis of previously conducted studies of morphological
447 features, described in detail various cell types of coelomocytes in 15 species from different
448 classes of echinoderms (Boolootain and Guise, 1958). The developed classification of formed
449 elements of the coelomic fluid amounted to at least 13 cell types. According to the authors,
450 different cell morphotypes in some cases reflected the functional state of cells of the same types.
451 The described cell elements are observed in all classes of echinoderms, except sea stars, in which
452 amoebocytes are considered to be the only cellular component of the immune system (Bossche,
453 1976).
454   Introduction of electron microscopy, histochemical, and histological methods has enabled
455 identification of five main cell types, the existence of which is now recognized by most
456 researchers: granular and agranular amoebocytes, morula cells, and lymphocyte-like and
457 flagellated cells (Korenbaum, 1989; Kudryavtsev, 2006). However, various names of the same
458 classes of starfish coelomocytes can still be found in the literature. Furthermore, genesis of
459 different cell types still remains unclear: whether they belong to several differentiation lines, or
460 they stem from common progenitor cells. The amount of different coelomocyte types in the
461 coelomic fluid depends on a wide range of external and internal factors, including different
462 techniques for coelomic fluid fixation, which may affect the formula of cellular composition
463 (Bossche and Jangoux, 1975).
464   The classification of adherent cells is even more ambiguous. It has been supposed that
465 small cells are progenitors of all other cell types and that irreversible transformation occurs upon
466 transition from small cells to differentiated cells, and from circulating cells with short
467 pseudopodia to flattened cells (Fontaine and Lambert, 1975; Bossche and Jangoux, 1975).
468 According to Pinsino (2007), adherent *Asteroidea* immune cells form cell shapes described as
469 petaloid or filopodial cytoplasmic protrusions, which replace each other through a series of
470 transitional forms for 8 min. In our study, cells with a small number of processes, which are
471 especially numerous at the 15th min of culturing, as well as insufficiently flattened cells of a 2-
472 minute culture may be assigned to the petaloid form. We describe for the first time the cell shape
473 with curved processes, which emerges after 60 min of culturing.
474   Each time group contains cells with petaloid and filopodial cytoplasmic protrusions. The
475 classification based on the most variable parameters distinguishing cell types with a high degree
476 of reliability enabled us to identify types of small and petaloid cells (type I) that represent the
477 initial and final stages of spreading across a cell substrate. These cells have the lowest, compared
478 to other types, area, a simple form and boundary microsculpture, and respectively, a low value of
479 the mean fractal dimension of the cell contour (outMeanD) and high Circularity. Type II is a

480 transitional type between the petaloid and filopodial forms, which is characterized by medium
481 values of most parameters. Type III includes predominantly cells of a filopodial form, which
482 may be called the most morphologically differentiated cell form. These cells have high values of
483 several fractal dimensions and lacunarities characterizing overall complexity of the cell shape
484 and inhomogeneity of space filling by the form, a large spreading area, and even a greater
485 spreading area of processes (low Density value), and a low Circularity value indicating
486 complexity of the overall shape of this cell type, which is the most different from the rounded
487 shape.
488   The identified cell types are comparable in each time group, but similar types differ in a
489 number of characteristics in different time groups, and comparison of these differences enables
490 identification of several trends in the dynamics of cell behavior. First of all, the degree of cell
491 spreading continues to significantly increase in all cell types during culturing for 1 hour. In this
492 case, the maximum activity of cells was observed at the fifth minute of culturing. Here, there is a
493 cell type (type 5-3) that significantly surpasses other types in microsculpture complexity and
494 overall complexity of the cell shape. This indicates cell motility, active process formation, and
495 cell shape changes. At this stage, cells are characterized by the search behavior; cell spreading
496 also occurs most rapidly. By the 15th min, activity of cells reduces. The number of processes
497 reduces; cells acquire a more rounded shape; the cell body area to protrusion area ratio increases;
498 the number of petaloid type cells increases. Despite continued cell spreading, it looks, according
499 to the patterns of morphological characteristics, like uniform spreading of a fixed cell with
500 pronounced retraction of processes and uniform filling of a substrate by the cell body. This is
501 confirmed by an increase in the cell area with a simultaneous reduction in most parameters that
502 characterize complexity of cell morphology. Morphological complexity of cells at the 60th min
503 of culturing decreases to a level comparable to that at the 2 min stage, but cells are characterized
504 by a significantly greater degree of spreading and symmetry. Curved processes, which develop in
505 this time group, make the cell shape more round, but do not reduce the Roundness parameter,
506 which distinguishes these cells from typical filopodial cells at other spreading stages where
507 increased protrusivity leads to a decrease in the Roundness value.
508

Conclusions

510   Unlike nerve tissue cells, the morphometry of which, both neurons (Pushchin and
511 Karetin, 2014), and microglia cells (Morrison et al., 2017; Young et al., 2018), is well developed,
512 and uses a wide range of nonlinear parameters in combination with different imaging methods,
513 the morphological description of fibroblast-like cells is less formalized. A large number of recent
514 studies on biochemical, morphological, physiological, and genetic processes associated with
515 changes in the immune cell behavior have used a statistically unverifiable language to describe
516 cell shapes. The difficulty is related to irregularity and a wide chaotic variety of shapes of
517 flattened cells. Attempt to cover the entire potential spectrum of cell shapes in vitro using
518 classical morphometry inevitably results in a set of rather general, non-specific, linear
519 morphometric parameters describing the general features of a two-dimensional object, such as

520 the area, diameter of the bounding circle, circularity, or elongation of the cell (Rajagopalan et al.,
521 2004; Solon et al., 2007). However, these structures can be effectively described by a set of
522 nonlinear morphometric parameters, including calculation of the fractal and information
523 dimension, evaluation of spatial heterogeneity and lacunarity of the object, its multifractal
524 spectrum, etc. A number of examples involving a wide range of cell types have demonstrated the
525 possibility, in principle, of efficient, comparative, numerical morphometry of cells (Karetin
526 2010a, 2010b; Karetin, 2016). This argues that the methodology based on the synthesis of linear
527 and nonlinear morphometry can effectively complement a non-formalized language for
528 description of morphology of invertebrates' immune cells in culture.
529   A complex statistical analysis of the morphology of coelomocytes from *Asterias*
530 *amurensis* (Echinodermata, Asteroidea), which included cluster and correlation analyses and an
531 variance analysis using a variety of linear and nonlinear cell morphology parameters, enabled
532 identification of cell characteristics, such as complexity of cell boundary microsculpture, overall
533 asymmetry of the cell, sizes of the cell, bounding circle, and convex hull, and inhomogeneity of
534 surrounding space filling by the cell and establishment of a relationship between these
535 characteristics and differences in the dynamics of cell spreading at different culturing stages.
536
537

538 **References**
539

540   Boolootain R and Guise A. 1958. Coelomic Corpuscles of Echinoderms. Biological
541 Bulletin 115:53–63.
542   Bossche Vanden JP and Jangoux M. 1976. Epithelial origin of starfish coelomocytes.
543 Nature 261:227-228.
544   Cerenius L, Söderhäll K. 2013. Variable immune molecules in invertebrates. Journal of
545 Experimental Biology 216: 4313-4319 DOI: 10.1242/jeb.085191.
546   Dommisse M, Hough D. 2004. http://www.environment.gov.au/resource/controlling-
547 northern-pacific-seastar-asterias-amurensis-australia.
548   Gordon AD. 1999. Classification, 2nd Edition. Boca Raton, London, New York,
549 Washington, DC: Chapman and Hall/CRC. ISBN 9781584880134.
550   Fisher WS. 1986. Structure and Functions of Oyster Hemocytes, in: Dr. Brehélin, M.
551 (Eds), Immunity in Invertebrates. Springer Verlag, Berlin, pp. 25–35. ISBN: 978-3-642-70770-4
552 (Print) 978-3-642-70768-1 (Online).
553   Fontaine AR and Lambert P. 1975. The fine structure of the leucocytes of the holothurian
554 Cucumaria miniata. Canadian Journal of Zoology 55:1530-1544.
555   Jangoux M. and Vanden Bossche JP. 1975. Morphologie et dynamique des coelomocytes
556 d'Asterias rubens L. (Echinodermata, Asteroidea). Forma et function 8:191-208.
557   Hine PM. 1999. The inter- relationship of bivalve haemocytes. Fish & Shellfish
558 Immunology 9:367-385 DOI: 10.1006/fsim.1998.0205.

559   Hwang S, Bang K, Lee J, Cho S. 2015. Circulating Hemocytes from Larvae of the
560   Japanese Rhinoceros Beetle Allomyrina dichotoma (Linnaeus) (Coleoptera: Scarabaeidae) and
561   the Cellular Immune Response to Microorganisms. PLoS ONE 10(6): e0128519
562   DOI:10.1371/journal.pone.0128519.
563   Karetin Yu. 2010. A comparative analysis of the nonlinear morphometry of in vitro
564   spread hemocytes in two bivalve species. Russian Journal of Marine Biology 36:429–434 DOI:
565   10.1134/S1063074010060040.
566   Karetin Yu. 2010. Comparative morphological analysis of in vitro cultured hemocytes
567   from two species of bivalve mollusks. Russian Journal of Marine Biology 36:367–372 DOI:
568   10.1134/S1063074010050068.
569   Karetin Yu. 2016. Nonlinear Analysis of the Morphology of Hemocytes from the Sea
570   Stars *Aphelasterias japonica* (Bell, 1881), *Patiria pectinifera* (Muller et Troschel, 1842), and the
571   Bivalve *Callista brevisiphonata* (Carpenter, 1864). Russian Journal of Marine Biology 42:315-
572   323 DOI: 10.1134/S1063074016040052.
573   Karetin Yu, Pushchin II. 2015. Analysis of the shapes of hemocytes of Callista
574   brevisiphonata in vitro (Bivalvia, Veneridae). Cytometry A 87:773-6 DOI: 10.1002/cyto.a.22676
575   Korenbaum ES. 1989. Ultrastructure of coelomocytes of Asterias amurensis starfish.
576   Tsitologiya 31:1165-1171.
577   Kudryavtsev IV. 2006. Immunoassay of protective reactions of Asterias rubens starfish.
578   PhD Dissertation, University of St. Petersburg. Available at http://medical-
579   diss.com/medicina/immunologicheskiy-analiz-zaschitnyh-reaktsiy-morskoy-zvezdy-asterias-
580   rubens.
581   Kurtz J. 2002. Phagocytosis by invertebrate hemocytes: Causes of individual variation in
582   Panorpa vulgaris scorpionflies. Microscopy Research and Technique 57(6):456-468 DOI:
583   10.1002/jemt.10099.
584   Kurucz E, Váczi B, Márkus R, Laurinyecz B, Vilmos P, Zsámboki J, Csorba K, Gateff E,
585   Hultmark D, Andó I. 2007. Definition of Drosophila hemocyte subsets by cell-type specific
586   antigens. Acta Biologica Hungarica 58:95-111. DOI: 10.1556/ABiol.58.2007.Suppl.8.
587   Martin GG, Hose Jo E. 1992. Vascular elements and blood (Hemolymph). Microscopic
588   Anatomy of Invertebrates 10:117-146.
589   Morrison H, Young K, Qureshi M, Rowe RK, Lifshitz J. 2017. Quantitative microglia
590   analyses reveal diverse morphologic responses in the rat cortex after difuse brain injury.
591   Scientific Reports 7:13211 DOI: 10.1038/s41598-017-13581-z.
592   Pinsino A, Thorndyke MC, Matranga V. 2007. Coelomocytes and post-traumaticresponse
593   in the common sea star Asterias rubens. Cell Stress Chaperones 12:331-341 DOI:
594   http://dx.DOI.org/10.1379/CSC-288.1.
595   Pushchin II, Karetin Yu. 2009. Retinal ganglion cells in the eastern newt Notophthalmus
596   viridescens: topography, morphology, and diversity. Journal of Comparative Neurology 516:533-
597   52 DOI: 10.1002/cne.22127.

598   Pushchin I, Karetin Yu. 2014. Retinal ganglion cells in the Pacific redfin, Tribolodon
599   brandtii dybowski, 1872: morphology and diversity. Journal of Comparative Neurology
600   522:1355-1372 DOI: 10.1002/cne.23489.
601   Rajagopalan P, Marganski WA, Brown XQ, Wong JY. 2004. Direct Comparison of the
602   Spread Area, Contractility, and Migration of balb/c 3T3 Fibroblasts Adhered to Fibronectin- and
603   RGD-Modified Substrata. Biophysical Journal 87:2818-2827 DOI:
604   10.1529/biophysj.103.037218.
605   Ratner S and Vinson SB. 1983. Phagocytosis and encapsulation: cellular immune
606   responses in Arthropoda. American Zoologist 23:185-194.
607   Ross DJ, Johnson CR, Chad L. 2002. Hewitt Impact of introduced seastars Asterias
608   amurensis on survivorship of juvenile commercial bivalves Fulvia tenuicostata. Marine Ecology
609   Progress Series 241:99-112 DOI: 10.3354/meps241099.
610   Scapigliatia G, Mazzinia M. 1994. In vivo and in vitro phagocytosis by hemocytes of the
611   stick insect Bacillus rossius. Bolletino di zoologia 61(2):115-120
612   DOI:10.1080/11250009409355869.
613   Schweitzer L, Renehan WE. 1997. The use of cluster analysis for cell typing. Brain
614   Research Protocols 1:100-8 DOI: 10.1016/s1385-299x(96)00014-1.
615   Sokolova EV, Karetin Yu, Davydova VN, Byankina AO, Kalitnik AA, Bogdanovich LN,
616   Yermak IM. 2016. Carrageenans effect on neutrophils alone and in combination with LPS in
617   vitro. Journal of Biomedical Materials Research Part A 104:1603-9 DOI: 10.1002/jbm.a.35693.
618   Solon J, Levental I, Sengupta K, Georges P, Janmey P. 2007. Fibroblast Adaptation and
619   Stiffness Matching to Soft Elastic Substrates. Biophysical Journal 93:4453-4461 DOI:
620   10.1529/biophysj.106.101386.
621   Stevens C. 2012. ISSG Database: Ecology of Asterias amurensis. Global Invasive
622   Species Database.
623   http://www.issg.org/database/species/ecology.asp?si=82&fr=1&sts=&lang=EN.
624   Stoepler TM, Castillo JC, Lill JT, Eleftherianos I. 2013. Hemocyte Density Increases
625   with Developmental Stage in an Immune-Challenged Forest Caterpillar. PLoS One 8(8):e70978
626   DOI: 10.1371/journal.pone.0070978 PMCID: PMC3735507.
627   Young K and Morrison H. 2018. Quantifying Microglia Morphology from
628   Photomicrographs of Immunohistochemistry Prepared Tissue Using ImageJ. Journal of
629   Visualized Experiments 136:e57648 DOI: 10.3791/57648.

Tukey-Kramer multiple comparison test of differences in 5 parameters in 4-time groups.

Area	Group	Mean	Different from groups
	2 min	45644.3	5 (P = 0,02401), 15 (P = 0,00000), 60 (P = 0,00000)
	5 min	63175.76	2 (P = 0,02401), 15 (P = 0,00000), 60 (P = 0,00000)
	15 min	88625.09	2 (P = 0,00000), 5 (P = 0,00000), 60 (P = 0,00000)
	60 min	151098.5	2 (P = 0,00000), 5 (P = 0,00000), 15 (P = 0,00000)
Circularity	**Group**	**Mean**	**Different from groups**
	5 min	0.1707483	15 (P = 0,00000), 2 (P = 0,00000), 60 (P = 0,00000)
	15 min	0.2614072	5 (P = 0,00000), 60 (P = 0,00873)
	2 min	0.290832	5 (P = 0,00000)
	60 min	0.2964816	5 (P = 0,00000), 15 (P = 0,00873)
Feret's diameter	**Group**	**Mean**	**Different from groups**
	2 min	1.078258	5 (P = 0,0000), 15 (P = 0,0000), 60 (P = 0,0000)
	5 min	1.520865	2 (P = 0,0000), 60 (P = 0,0000)
	15 min	1.584021	2 (P = 0,0000), 60 (P = 0,0000)
	60 min	2.144441	2 (P = 0,0000), 5 (P = 0,0000), 15 (P = 0,0000)
in50_out50	**Group**	**Mean**	**Different from groups**
	15 min	1.328015	60 (P = 0,00003), 5 (P = 0,00000)
	2 min	1.486176	60 (P = 0,04257), 5 (P = 0,00000)
	60 min	1.797293	15 (P = 0,00003), 2 (P = 0,04257), 5 (P = 0,00082)
	5 min	2.222238	15 (P = 0,00000), 2 (P = 0,00000), 60 (P = 0,00082)
LE	**Group**	**Mean**	**Different from groups**
	60 min	1.709738	15 (P = 0,00000), 5 (P = 0,00000), 2 (P = 0,00000)
	15 min	2.075289	60 (P = 0,00000), 5 (P = 0,00025), 2 (P = 0,00000)
	5 min	2.296859	60 (P = 0,00000), 15 (P = 0,00025), 2 (P = 0,01327)
	2 min	2.473771	60 (P = 0,00000), 15 (P = 0,00000), 5 (P = 0,01327)

2
3
4
5
6
7

Figure 1

Silhouette images of cells at different stages of cultivation: A – 2 min. (group 1); B – 5 min. (group 2); C – 15 min. (group 3); D – 60 min. (group 4).

A
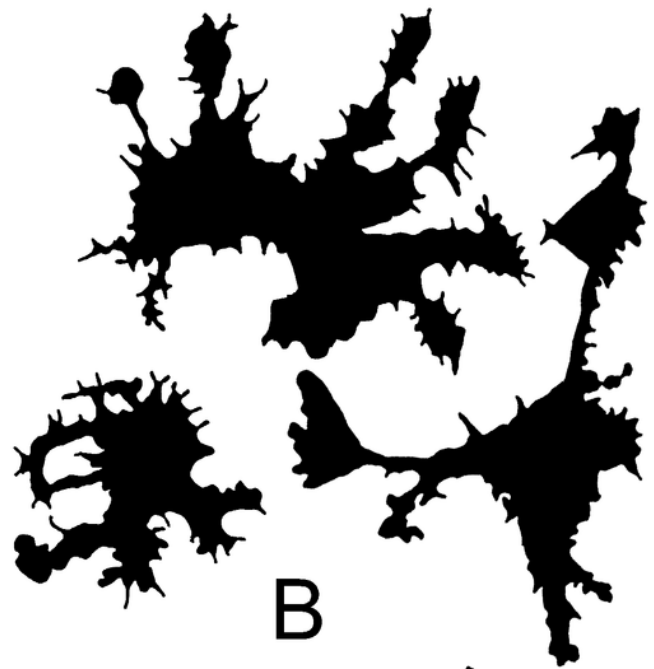
B
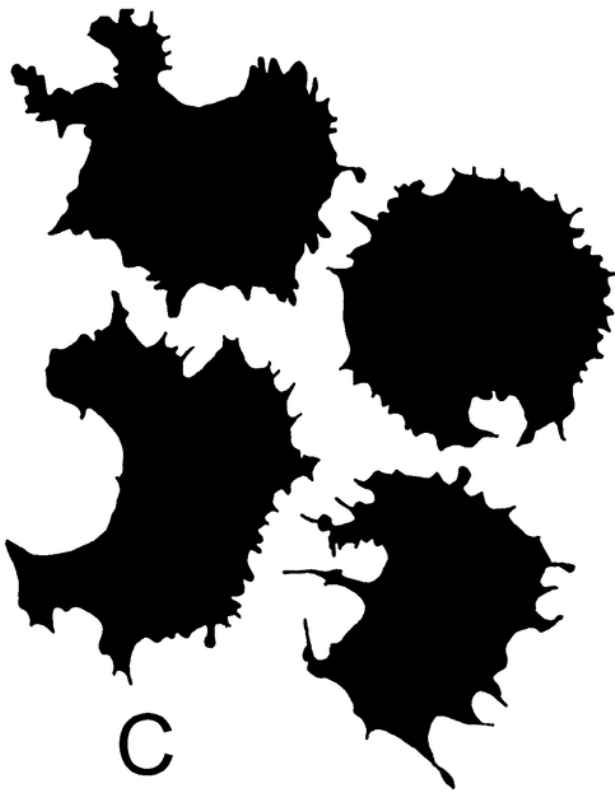
C

D

Figure 2

Different trends in changes in parameter values during in vitro culturing of coelomocytes from A. amurensis. A – area; B – Circularity; C - Feret's Diameter; D - Mean Local Connected Fractal Dimension of contour images of cells; E - in50/out50.

A

B

C

D

E

○— Mean
□ St. error of mean
⊥ Conf. intervals
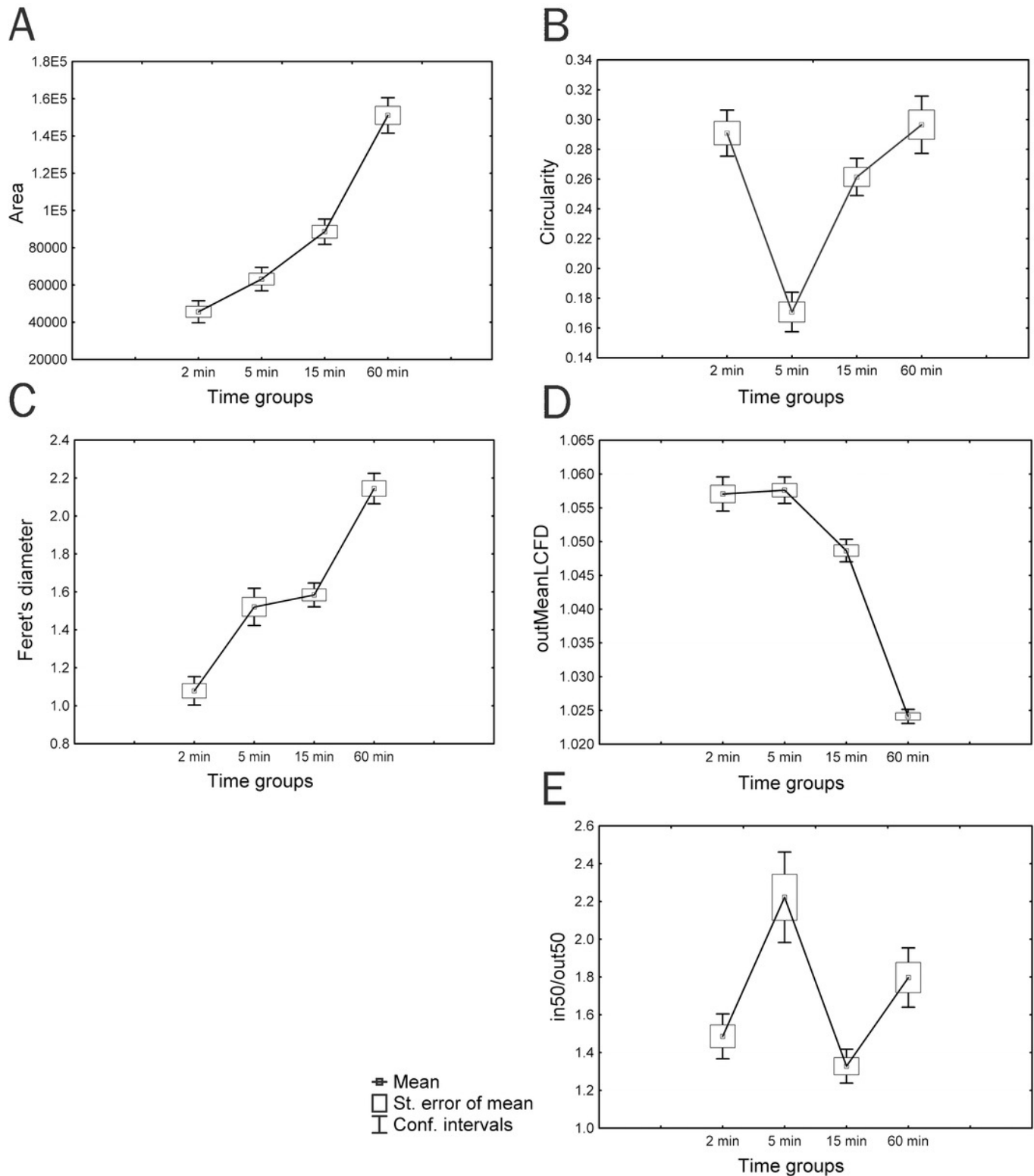
Figure 3

Convex hull of cell.
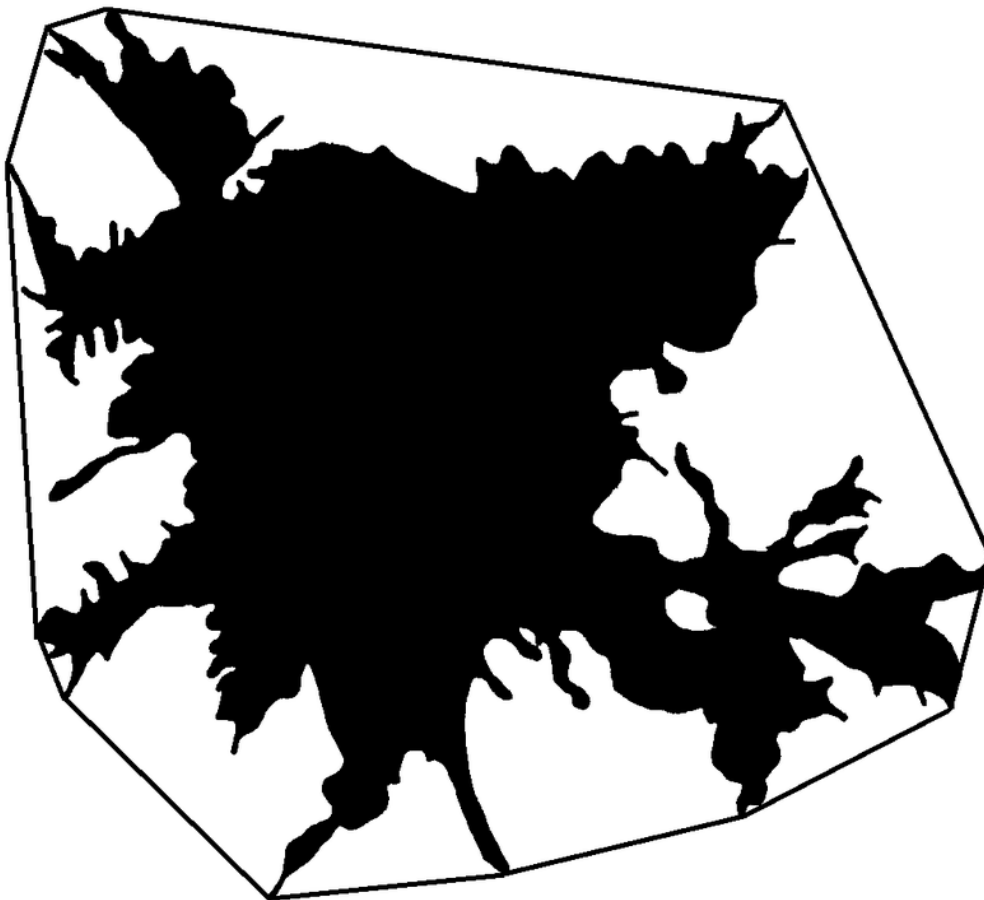
Figure 4

1/2half and *in50/out50* calculation. 1/2half = A/B , where A, B – two segments of the cell lying in different halves of the bounding circle . in50/out50 = C/D, where C and D are the parts of the cell located in the inner and outer part of the
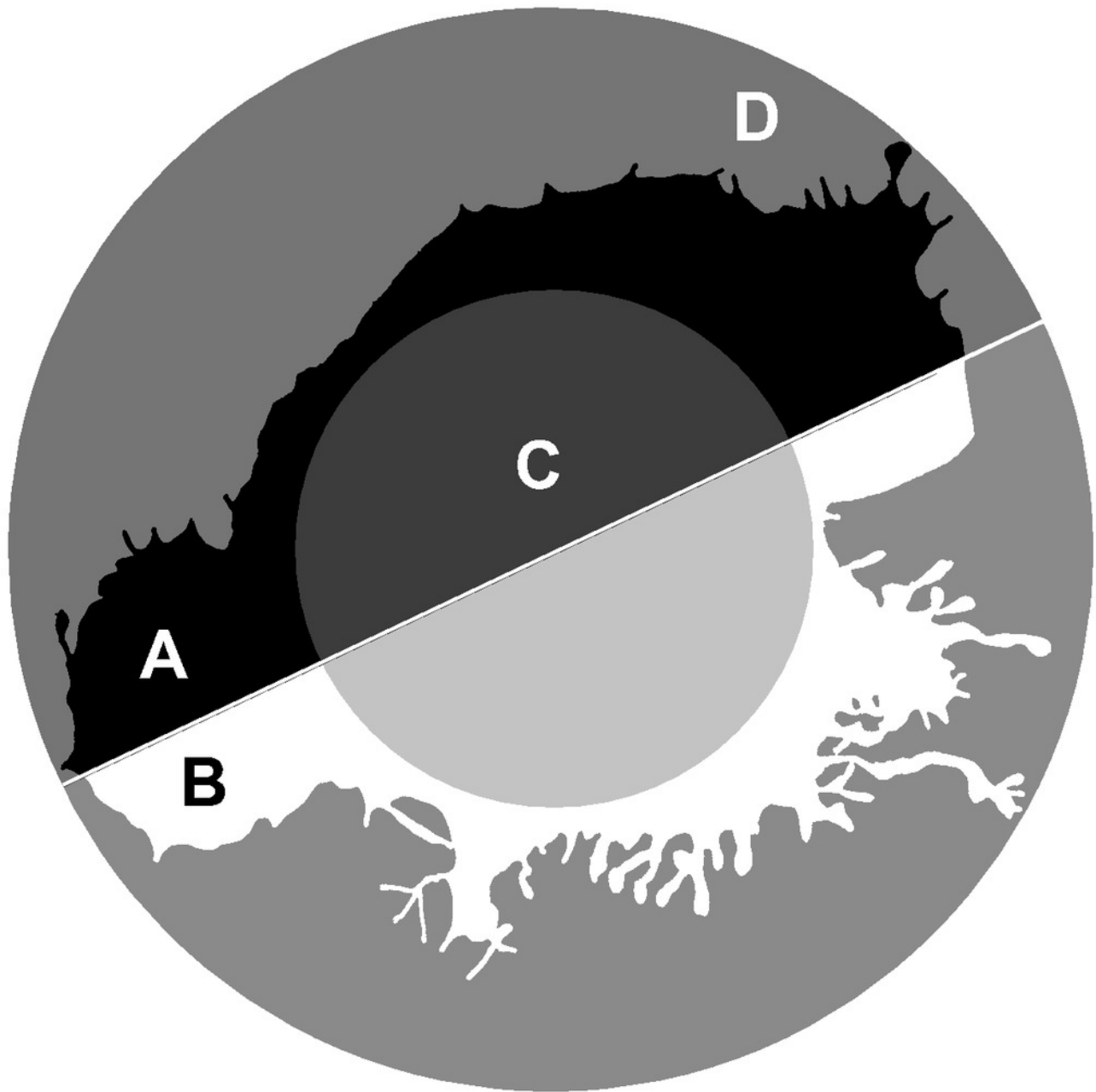
Figure 5

Box-counting fractal dimension calculation. See the description of the method in the text.
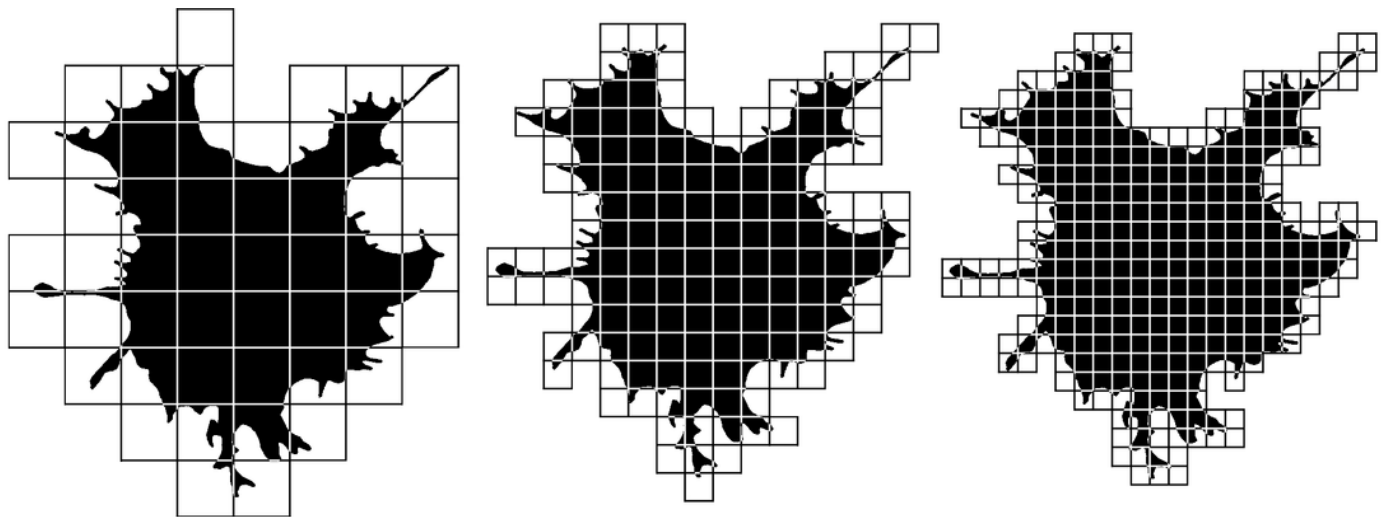
Figure 6

Cluster diagrams for 4 time groups, plotted using Area, Circ, Feret, in50/out50, and LE parameters: A. – 2 min.; B. – 5 min.; C. – 15 min.; D. – 60 min. Ward`s method, Euclidean distance measure.
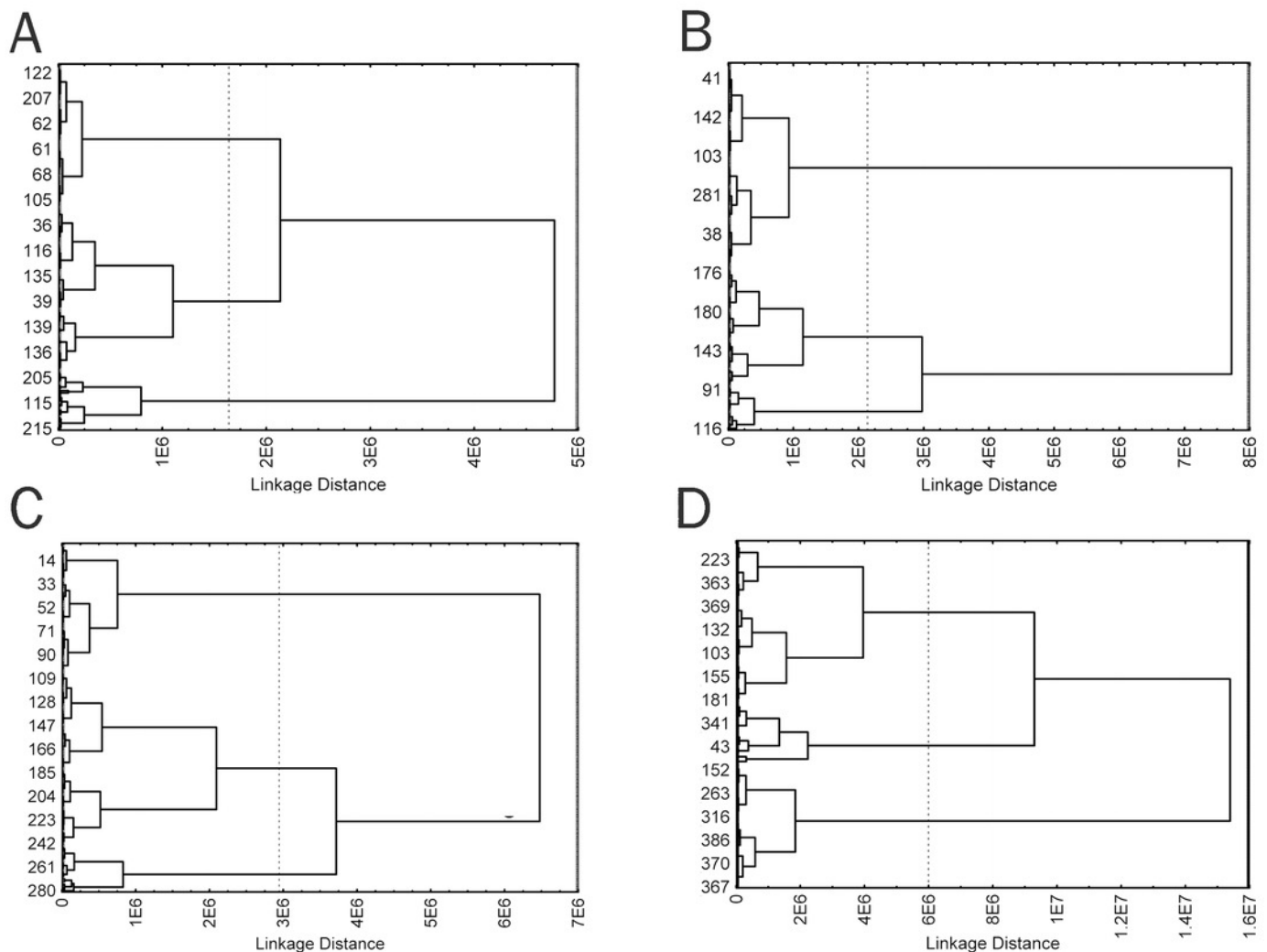
Figure 7

. Silhouette images of type I − III cells from all time groups.
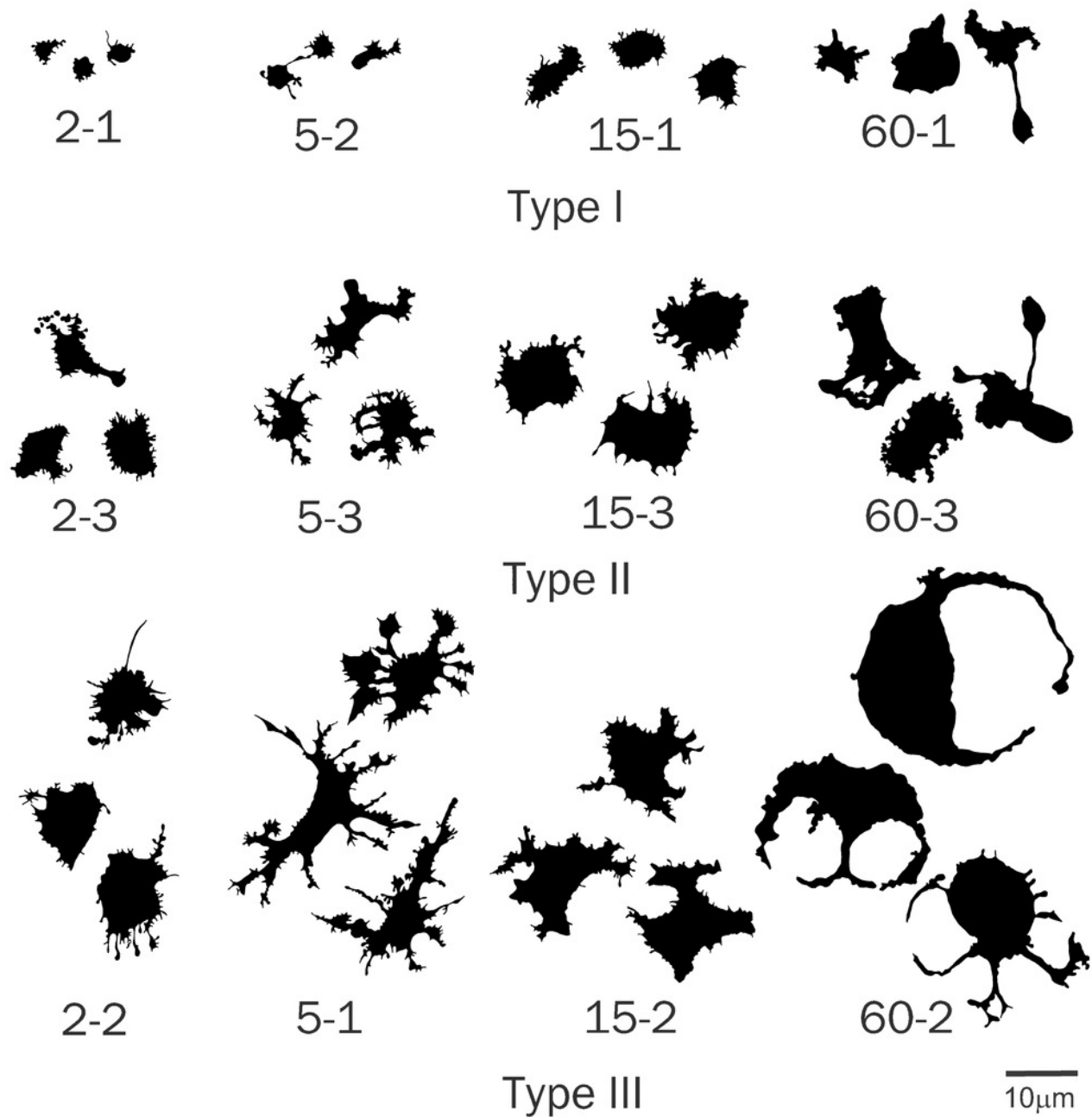
Figure 8

Plots of means and 95% confidence intervals for parameters of identified cell types: A – Area, B – Feret's Diameter, C – Perimeter, D – Hull's Perimeter, E – Roundness.

A

B

C

D

E

Mean
St. error of mean
Conf. intervals
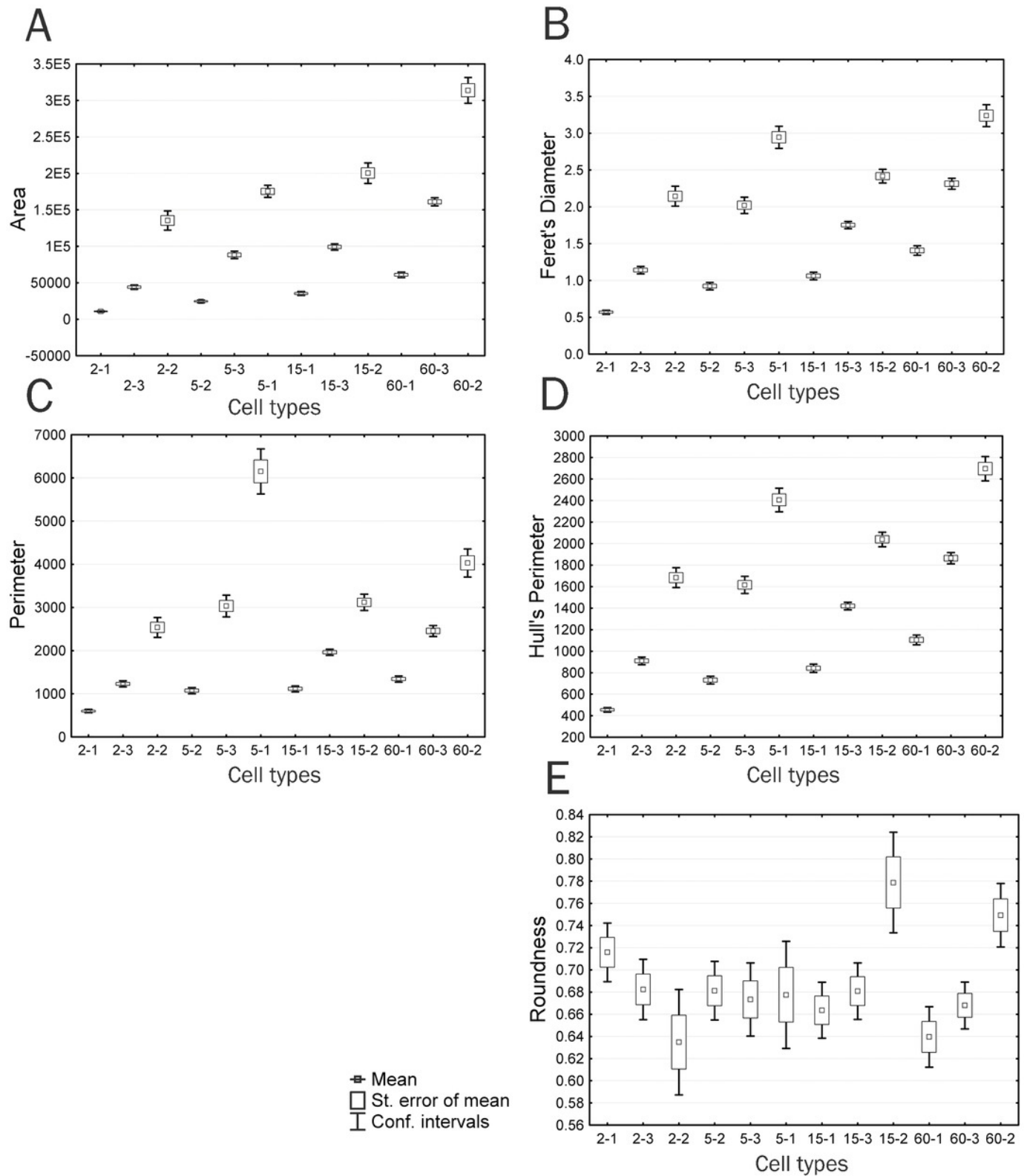
Figure 9

Cell morphology corresponding to the different values of outMeanD and outMeanLFD parameters.